Phase modulation with micromachined resonant mirrors for low-coherence fiber-tip pressure sensors

X. M. Zhang[1], Yuxiang Liu[2], H. Bae[2], C. Pang[2] and M. Yu[2,*]

[1]*Department of Applied Physics, Hong Kong Polytechnic University, Hung Hom, Kowloon, Hong Kong S.A.R., China*
[2]*Department of Mechanical Engineering, University of Maryland, 2132 Martin Hall, College Park 20742, USA*
**mmyu@umd.edu*

Abstract: This letter presents a simple phase modulation scheme for interrogation of low-coherence interferometry based fiber-tip pressure sensors to enable real-time monitoring and miniaturization of the entire sensor system. The key idea is to introduce a sinusoidal modulation signal and retrieve the sensing cavity length change using a simple algorithm, without resorting to any time information. In experiments, phase modulation has been achieved by using a silicon-micromachined tunable Fabry-Pérot interferometer, which is integrated with a light source and a photodiode onto a single chip. Compared with the conventional interrogation methods, this scheme possesses the merits of being less susceptible to disturbance, easy control and easy miniaturization, making it particularly suitable for sensing in constrained spaces and harsh environments.

OCIS codes: (060.2370) Fiber optics sensors; (120.5050) Phase modulation; (120.5475) Pressure measurement; (120.3180) Interferometry.

References and links

1. J. Xu, X. Wang, K. L. Cooper, and A. Wang, "Miniature all-silica fiber optic pressure and acoustic sensors," Opt. Lett. **30**(24), 3269-3271 (2005).
2. Y. Zhu, Z. Huang, F. Shen and A. Wang, "Sapphire-fiber-based white-light interferometric sensor for high-temperature measurements," Opt. Lett. **30**(7), 711-713 (2005).
3. W. N. MacPherson, J. M. Kilpatrick, J. S. Barton, and J. D. Jones, "Miniature fiber optic pressure sensors for turbomachinery applications," Rev. Sci. Instrum. **70**(3), 1868-1874 (1999).
4. J. I. Peterson and G. G. Vurek, "Fiber-optic sensors for biomedical applications," Sci. **224**(4645), 123-127 (1984).
5. S. Nesson, M. Yu, X. M. Zhang, and A. H. Hsieh, "Miniature fiber optic pressure sensor with composite polymer-metal diaphragm for intradiscal pressure measurements," J. Biomed. Opt. **13**(4), 044040 (2008).
6. K. Totsu, Y. Haga, and M. Esashi, "Ultra-miniature fiber-optic pressure sensor using white light interferometry," J. Micromech. Microeng. **15**(1), 71-75 (2005).
7. Y. J. Rao, "Recent progress in fiber-optic extrinsic Fabry-Pérot interferometric sensors," Opt. Fiber Technol. **12**(3), 227-237 (2006).
8. V. Bhatia, K. A. Murphy, R. O. Claus, M. E. Jones, J. L. Grace, T. A. Tran and J. A. Greene, "Optical fiber based absolute extrinsic Fabry-Pérot interferometric sensing system," Meas. Sci. Technol. **7**(1), 58-61 (1996).
9. E. Cibula and D. Đonlagic, "Miniature fiber-optic pressure sensor with a polymer diaphragm," Appl. Opt. **44**(14), 2736-2744 (2005).
10. Y. Zhu and A. Wang," Miniature Fiber-Optic Pressure Sensor," IEEE Photon. Technol. Lett. **17**(2), 447-449 (2005).
11. Y. Wang, M. Han, and A. Wang, "High-speed fiber-optic spectrometer for signal demodulation of inteferometric fiber-optic sensors," Opt. LETT. **31**(16), 2408-2410 (2006).
12. Y. Wang, M. Han and A. Wang, "Analysis of a high-speed fiber-optic spectrometer for fiber-optic sensor signal processing," Appl. Opt. **46**(33), 8149-8158 (2007).
13. B. T. Meggitt , "Fiber optic white light interferometric sensors," in *Optical Fiber Sensor Technology – Fundamentals*, K. T. V. Gratten and B. T. Meggitt, eds. (Kluwer, 2000), pp. 205-214.
14. K. J. Gåsvik, *Optical Metrology, 2nd ed.* (John Wiley & Sons, 1995).

#116807 - $15.00 USD Received 8 Sep 2009; revised 19 Oct 2009; accepted 21 Oct 2009; published 16 Dec 2009

15. Y. J. Rao and D. A. Jackson, "Prototype fiber-optic-based Fizeau medical pressure sensor that uses coherence reading," Opt. Lett. **18**(24), 2153-2155 (1993).
16. M. Adachi, "Phase-shift algorithm for white-light interferometry insensitive to linear errors in phase shift," Opt. Rev. **15**(3), 148–155 (2008).
17. M. Yu and B. Balachandran, "Acoustic measurements using a fiber optic sensor system", J. Intell. Mat. Syst. Struct. **14**(7), 409-414 (2003).
18. C-S Kang, J-A Kim,T. B. Eom, R. Jang, H. Y. Park, and J. W. Kim, "High speed phase shifting interferometry using injection locking of the laser frequency to the resonant modes of a confocal Fabry-Perot cavity," Opt. Exp. **17**(3), 1442-1446 (2009).
19. M. Schmidt, B. Werther, N. Fürstenau, M. Matthias, and T. Melz, "Fiber-Optic Extrinsic Fabry-Perot Interferometer Strain Sensor with < 50 pm displacement resolution using three-wavelength digital phase demodulation," Opt. Exp. **8**(8), 475-480 (2001).
20. J. M. Kilpatrick, W. N. MacPherson, J. S. Barton, and J. D. C. Jones, "Phase-demodulation error of a fiber-optic Fabry–Perot sensor with complex reflection coefficients," App. Opt. **39**(9), 1382-1388 (2000).
21. W. N. MacPherson, S. R. Kidd, J. S. Barton, and J. D. C. Jones, "Phase demodulation in optical fibre Fabry-Perot sensors with inexact phase steps," IEE Proc.-Optoelectron. **144**(3), 130-133 (1997).
22. R. Legtenberg, A. W. Groeneveld and M. Elwenspoek, "Comb-drive actuators for large displacements," J. Micromech. Microeng. **6**(3), 320–329 (1996).
23. A. Dubois, "Phase-map measurements by interferometry with sinusoidal phase modulation and four integrating buckets," J. Opt. Soc. Am. A **18**(8), 1972-1979 (2001).
24. J. H. Cole, B. A. Danver, and J. A. Bucaro, "Synthetic-heterodyne interferometric demoludation," IEEE J. Quantum Electron. QE-18(4), 694-697 (1982).
25. A. Dandridge, A. B. Tveten, and G. Giallorenzi, "Homodyne demodulation scheme for fiber optic sensor using phase generated carrier," IEEE Trans. Microwave Theory Tech. **MTT-30**(10), 1635-1641 (1982).
26. M. J Connelly, "Digital synthetic-heterodyne interferometric demodulation," J. Opt. A: Pure Appl. Opt. **4**(6), S400–S405 (2002).
27. M. J. Connelly, P. Szecowka, R. Jallapuram, S. Martin, V. Toal and M. P. Whelan, "Laser Doppler vibrometry system using the synthetic-heterodyne interferometric demodulation scheme implemented on a CMOS DSP camera," in *Proceedings of Sixth International Symposium, Communication Systems, Networks and Digital Signal Processing*, E. Leitgeb, W. Kogler, Z. Ghassemlooy, eds. (Graz, Austria, 2008), pp. 133-136.
28. S-C Huang and H. Lin, "Modified phase-generated carrier demodulation compensated for the propagation delay of the fiber," Appl. Opt. **46**(31), 7594-7603 (2007).
29. L. Feng, J. He, J-Y Duan, F. Li, and Y-L Liu, "Implementation of phase generated carrier technique for FBG laser sensor multiplexed system based on Compact RIO," J. Electron. Sci. Technol. China **6**(4), 385-388 (2008).

1. Introduction

Fiber-tip pressure sensors refer to the fiber-optic sensors that construct an extrinsic Fabry-Pérot (FP) cavity between the tip of an optical fiber and an external mirror. They have recently received considerable attention due to the demands of pressure monitoring in constrained spaces and harsh environments such as turbo engines [1-3] and human organs [4-6]. Although miniature pressure sensors have been reported in literature, some emerging advanced applications may not only require the pressure sensors to be small enough to reach the regions of interest, but also require the entire sensing system (including both the pressure sensors and the interrogation subsystems) to be miniaturized to facilitate in-situ pressure sensing [7]. These applications include pressure measurements on rotary blades, in-situ pressure monitoring carried out with micro air/underwater vehicles, and implantable or portable medical pressure monitoring devices. For these applications, easy miniaturization, simple implementation, real-time and reliable measurements become the major concerns. Therefore, the control and signal processing should be as simple as possible, the response speed should be fast enough to respond to quasi-static pressure changes (typically < 100 Hz), and the interrogation method should be robust in the presence of noise and disturbance.

To interrogate the cavity length change of the sensors in response to the external pressure, various methods have been demonstrated. Low-coherence interferometry (LCI) has gained increasing popularity as it enables absolute distance measurements [8] while suppressing the influences of parasitic cavities and light source instability (e.g., wavelength drift and power fluctuations) [7]. Most of the reported LCI-based fiber-tip pressure sensors utilized spectrometers or optical spectrum analyzers to obtain the reflection (or transmission) spectrum

#116807 - $15.00 USD Received 8 Sep 2009; revised 19 Oct 2009; accepted 21 Oct 2009; published 16 Dec 2009

of the sensing cavity, and the cavity length change is retrieved by using the peak tracking technique [5-7, 9, 10]. The use of spectral information presents significant impediments to both the miniaturization and the response speed. Although high-speed fiber-optic spectrometers have been reported recently [11, 12], miniaturization of these spectrometers still remains a challenge. Advanced techniques such as linear demodulation method and phase shifting method could be incorporated into the sensor interrogation [13, 14], which enable fast detection speed and easy data retrieval by utilizing the optical power signal (not spectral signal). However, the linear demodulation method requires the sensor to be operated at a quadrature point and thus real-time stabilization of the operating condition is needed. The phase shifting method introduces additional phase changes in a controllable manner, usually a linear phase ramp [15] or several well-defined phase steps [16-21]. It requires sophisticated control of the phase steps and strict synchronization between the modulation and sampling [13-21].

In this letter, we propose and demonstrate a phase modulation scheme that can be used in a single-chip integrated LCI sensor system for real-time pressure monitoring. Such scheme introduces a sinusoidal phase modulation with an amplitude (i.e., modulation depth) equal to or slightly greater than π. The sensing cavity length can be retrieved from the power levels of some extremum points in the modulated output waveform. The scheme is implemented by using a microfabricated tunable FP filter. The details of this scheme and its advantages and uniqueness will be discussed as follows.

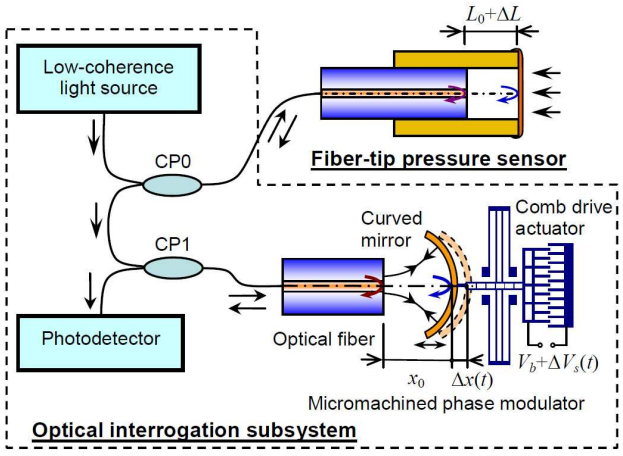

Fig. 1. Schematic setup of sinusoidal phase modulation scheme for low-coherence interrogation of the fiber-tip pressure sensors. CP0 and CP1 represents 1 × 2 optical couplers.

2. Design and working principle

The configuration of the entire sensor system (including a fiber-tip pressure sensor and an optical interrogation subsystem) for incorporating the sinusoidal phase modulation scheme is shown in Fig. 1. A low-coherence light first passes a 2 × 1 optical coupler (CP0) before entering the FP sensing cavity of the pressure sensor. The reflected light then goes to the reference interferometer, which employs a tunable FP cavity formed by a cleaved fiber end as a partial mirror and a micro-fabricated curved mirror as another mirror. The curved mirror can be driven by an electrostatic comb drive actuator to facilitate a tunable cavity length of the reference interferometer. The reflected light from the reference interferometer is transmitted to a photodetector for optical power detection. Initially, the reference cavity length can be adjusted to a desired level by applying a static bias voltage V_b. The dynamic phase modulation can be achieved conveniently by driving the curved mirror in resonance with a modulation voltage $\Delta V_s(t) = V_{s0}\cos(2\pi f_0 t)$, where V_{s0} represents the amplitude of modulation voltage, t is

#116807 - $15.00 USD Received 8 Sep 2009; revised 19 Oct 2009; accepted 21 Oct 2009; published 16 Dec 2009

the time and f_0 is the resonant frequency of the curved mirror. The use of resonant oscillation can produce enough displacement (> $\lambda/2$) with a small modulation voltage (~ 0.1 V) even though the actuator may need a stiff support for higher f_0. It is noted that the modulation frequency is not limited to the resonance. The sensor system can work well at other modulation frequencies beyond or below the resonance as long as the displacement of the curved mirror is large enough.

Based on the output optical power of LCI [13] and the vibrational response of comb drive actuator [22], the normalized output power can be expressed as

$$P(\tau) = 1 + T_0 \cos\left(A \sin\tau + \phi_0'\right). \tag{1}$$

here τ is the normalized time and $\tau = 2\pi f_0 t$. T_0 is the temporal coherence function and it can be regarded as a constant when the cavity length change is small. The variable A represents the modulation depth and ϕ_0' stands for the optical phase to be determined. They are related to the basic parameters by

$$A = \frac{4\pi\varepsilon_0 Nh}{\lambda_0 \zeta K_0 g} \cdot V_b V_{s0}, \tag{2a}$$

$$\phi_0' = \frac{4\pi}{\lambda_0}\Delta L + \frac{4\pi}{\lambda_0}\left[L_0 - x_0 + \frac{\varepsilon_0 Nh}{g}\left(V_b^2 + \frac{1}{2}V_{s0}^2\right)\right], \tag{2b}$$

where ε_0 is the permittivity of air, N the comb finger number, h the depth of comb finger, g the comb finger gap, K_0 the system stiffness and ζ the damping factor of the vibrational mirror. L_0 and x_0 are the initial lengths of sensing and reference cavity, respectively. ΔL is the change of sensing cavity length in response to the external pressure (see Fig. 1). On the right side of Eq. (2b), the second term could be set to be 0 by proper choices of V_b and V_{s0} in the initial biasing so that it yields $\phi_0' = 4\pi\Delta L/\lambda_0$. In this way, ϕ_0' becomes solely dependent on ΔL.

The expression in Eq. (1) is valid based on two assumptions. One is $\zeta V_{s0}/6V_b << 1$ (namely, small-modulation assumption). Under this condition, the harmonic response term $\sin(2\tau)$ becomes negligible and thus does not appear in Eq. (1). The other assumption is that the external pressure is quasi-static, that is, the highest frequency component of sensor response is much slower than the modulation frequency (namely, quasi-static assumption). According to Eq. (1), if $A > \pi$, the total phase $\left(A\sin\tau + \phi_0'\right)$ would experience a change more than 2π over one period of modulation. As a result, all the extremum points would appear during the modulation (to be discussed later). The output waveform is exemplified in Fig. 2 with the values $T_0 = 1$, $A = 1.1\ \pi$ and $\phi_0' = \pi/3$. It can be observed that the waveform has a ditch and a hump, whose local extrema occur at $\tau = -\pi/2$ and $+\pi/2$, respectively. The corresponding powers are noted as $P_{-\pi/2}$ and $P_{+\pi/2}$. Another feature observed from Fig. 2 is that there exist two symmetric maximum power points with respect to $\tau = -\pi/2$ and similarly two symmetric minimum power points with respect to $\tau = +\pi/2$. The corresponding powers are represented by P_{max} and P_{min}, respectively. All these featured points can be verified by solving $dP/d\tau = 0$. In parametric study, the influences of A and ϕ_0' on the shape of output waveform are examined. It is observed that the value of A determines the relative position of the ditch and the hump in the vertical direction. If $A \geq \pi$, the power values corresponding to the local minimum of the ditch and the local maximum of the hump start to overlap (i.e., $P_{-\pi/2} \leq P_{+\pi/2}$). This feature of the waveform can be used in experiment to observe whether the modulation depth is large enough. With the variation of ϕ_0', the local extrema of the ditch and hump move up or down at the same pace. When A goes larger so that the total phase $\left(A\sin\tau + \phi_0'\right)$is beyond 2π, the features of waveform become more complicated and messy.

#116807 - $15.00 USD Received 8 Sep 2009; revised 19 Oct 2009; accepted 21 Oct 2009; published 16 Dec 2009

This is why the modulation depth is required to be larger than π but preferably only by a small amount. It is worth noting that this choice does not restrict the dynamic range of sensor response as it is not necessary to maintain $A+\phi' \le 2\pi$ (in one period of modulation, the term $A\sin\tau+\phi_0'$ is changed from $-A+\phi_0'$ to $+A+\phi_0'$, the range remains to be 2*A* regardless of the value of ϕ_0').

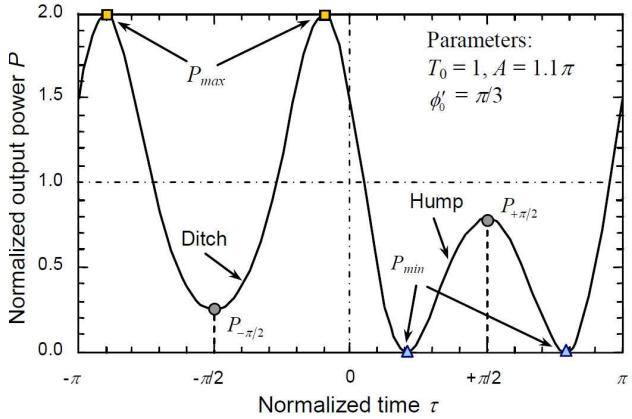

Fig. 2. Featured points on the modulated output waveform.

To retrieve ϕ_0' from the received continuous waveform without resorting to any time information, both ϕ_0' and *A* can be determined simultaneously by

$$\cos(-A+\phi_0') = \frac{2P_{-\pi/2} - P_{\max} - P_{\min}}{P_{\max} - P_{\min}}, \tag{3a}$$

$$\cos(A+\phi_0') = \frac{2P_{+\pi/2} - P_{\max} - P_{\min}}{P_{\max} - P_{\min}}. \tag{3b}$$

The solutions of ϕ_0' and *A* could have multiple values due to the inverse trigonometric functions. As the value of *A* is preset to be slightly larger than π, this restriction helps determine the ranges of inverse cosine solutions and thus the values of ϕ_0' and *A* can be determined without ambiguity. A detailed discussion can be found in Appendix. As the values of ϕ_0' and *A* are calculated by subtraction and division of the power levels of the extrema (see Eqs. (3a) and (3b)), the common background noise of LCI output is eliminated and thus the fluctuation of light source power does not affect the result. As compared to the linear demodulation method and the phase shifting method [13-17, 21], this algorithm offers some additional advantages, for instance, it does not rely on the time information of the waveform and thus avoids the needs of synchronization and time control. As both ϕ_0' and *A* can be determined simultaneously, it does not require a pre-calibration of the modulation depth and thus tolerates modulation signal drift during the operation. This is very convenient to practical uses and makes it suitable for harsh environment where strong noise and drift of operational conditions may exist. Moreover, the data processing is relatively simple as it just keeps picking the extrema from the continuous output waveform, without need for filtering processes in the time or frequency domain. In experimental implementation, the extremum picking can be realized based on two procedures. First, the output data stream is continuously differentiated to find the zero-crossing point, which indicates the appearance of an extremum. Second, the sequence of appearance of the extrema is already known to be in the sequence of maximum, ditch bottom, maximum, minimum, hump top, and minimum (see Fig. 2). Once the

#116807 - $15.00 USD Received 8 Sep 2009; revised 19 Oct 2009; accepted 21 Oct 2009; published 16 Dec 2009

first maximum is found, the identities of all the following extrema can be determined. As the extremum picking is continuous, in this sense, the sensor measurement is in real time.

Indeed, similar sinusoidal modulation has been investigated for other purposes in LCI-based applications such as temporal fringe processing [13, 15] and surface mapping using phase-shifting interferometers [23]. The former employs complicated digital filters in the time and spectral domains [15]. The latter separates one modulation period into four quarters and integrates the optical power during the time interval of each quarter [23]. Both methods require fixed modulation depth and frequency, and enforce strict synchronization and precise time control. By contrast, the proposed scheme in this letter offers a much simpler solution. In the conventional laser-based interferometric sensors, similar phase modulation has also been studied in phase-generated carrier (PGC) technique [24-29]. Periodic phase modulation is introduced by oscillating a piezoelectrically driven mirror or by altering the laser wavelength. The expression of the output power has the similar form to Eq. (1). To demodulate the phase term ϕ_0', the interferometric signal is expanded in Bessel functions to separate into three parts: the DC signal, one dependent on $\sin\phi_0'$ and another on $\cos\phi_0'$. After the signal goes through subsequently low-pass filters, differentiation, cross-multiplication, subtraction and integration, the phase term ϕ_0' can be obtained without involving any trigonometric or inverse trigonometric functions. It demonstrates the advantages of high sensitivity and large dynamic range, but it requires cumbersome computation (not in real time) and fixed modulation frequency/depth. Most of the early implementations used analog circuits [24, 25]. Recently studies using digital signal processing have found the PGC is susceptible to quantization noise, laser intensity noise, and second-harmonic distortion [26]. For these reasons, the PGC technique is not very suitable for the practical applications.

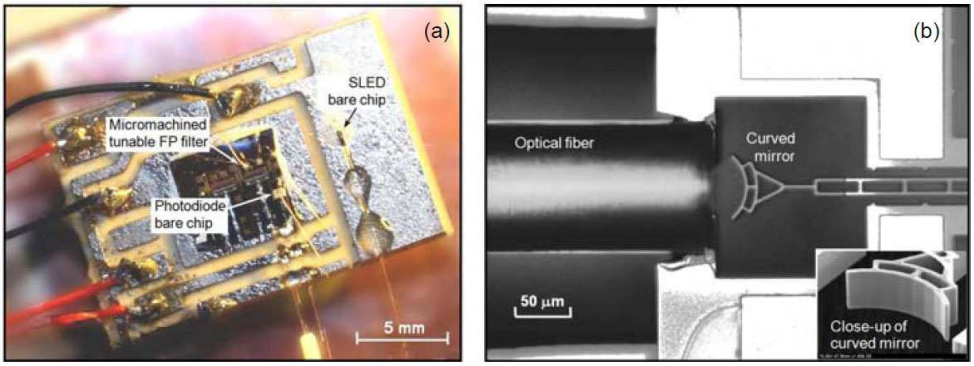

Fig. 3. Single-chip integrated optical interrogation subsystem for implementation of the sinusoidal phase modulation scheme. (a) Photograph of the chip; and (b) micrograph of the micromachined resonant mirror, with a close-up of the mirror shown in the inset.

3. Experimental verification

In experimental implementation, the sinusoidal phase modulation scheme is incorporated into a miniature optical interrogation subsystem as shown in Fig. 3(a), which integrates a micromachined tunable FP filter, a superluminescent light emitting diode (SLED) bare chip, and a photodiode bare chip onto a single substrate, together with all the necessary electrical and fiber connections. The micromachined tunable FP filter serves as the phase modulator, which employs a curved mirror driven by a comb drive actuator as shown in Fig. 3(b) and the inset. The micromachined structures are fabricated by deep reactive ion etching using a silicon-on-insulator wafer (structural layer 25 μm thick). The curved mirror has a radius of 39 μm, slightly smaller than the sensing cavity length (designed value 40 μm) to facilitate the initial bias. The effective reflectivity is measured to be approximately 4%, yielding a good visibility in the interferometric output. Under static actuation, the curved mirror moves away

#116807 - $15.00 USD Received 8 Sep 2009; revised 19 Oct 2009; accepted 21 Oct 2009; published 16 Dec 2009

from the fiber end by $\Delta x = 0.028V^2$ μm (V is the static voltage in unit of volt). The resonant frequency measures 2.4 kHz, more than 20 times higher than the targeted maximum frequency components of the pressure field (100 Hz). Thus the quasi-static relation is satisfied. The air damping factor is approximately 0.013. As it has $\zeta V_{s0}/6V_b \approx 3\times10^{-4} << 1$, the small-modulation assumption is valid.

The fiber-tip pressure sensor is prepared using the same procedures developed in our previous work [5]. It consists of a polymer-metal composite diaphragm, a single mode fiber, and a glass tube. The glass tube acts as a housing structure to hold the diaphragm and to allow for the insertion of the optical fiber. The fiber has a well-cleaved end-face, serving as a partial mirror of a Fabry-Pérot cavity; while the reflective diaphragm serves as another mirror. The fabricated sensor has an outer diameter of only 366 μm, making it suitable for many applications that have constrained spaces. In experiment, the pressure sensor is characterized in a pressure chamber. Under the initial atmospheric pressure, V_b and V_{s0} are chosen to be 1.2 V and 0.18 V, respectively. The waveforms of the modulation voltage and the interferometric output are shown in the channels 1 and 2 of Fig. 4. The modulation depth A is approximately 1.05π. As the external pressure is increased gradually, the local extrema of the ditch and the hump move down at the same pace in response to the shortening of the sensing cavity. Such behavior agrees well with the theoretical prediction. At a pressure level of 1.5 kPa, the output waveform is shown in the channel 3 of Fig. 4. According to Eqs. (3a) and (3b), it can be calculated that the sensing cavity experiences a length change of 70 nm. For the calibration purpose, the static sensor responses are also measured by tracking the peaks of the reflection spectrum by using an optical spectrum analyzer (Ando AQ6319) in the absence of the reference cavity. The results obtained with the two methods are plotted in Fig. 5. In both measurements, the cavity length decreases almost linearly with respect to the pressure. The linear approximations are obtained to be $\Delta L = -0.046P$ for the sinusoidal phase modulation scheme and $\Delta L = -0.048P$ for the reflection spectrum method. Here P is the gauge pressure with a unit of kPa and ΔL is the cavity length change with a unit of μm. It can be seen that the results match closely with a discrepancy of about 4%.

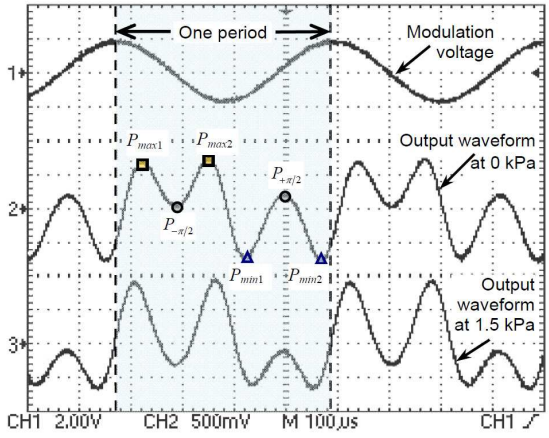

Fig. 4. Measured waveforms of the modulation voltage signal applied to the micromachined resonant mirror and the interferometric outputs in response to different external pressures.

To investigate the influence of the modulation depth, the pressure sensor is subjected to a constant pressure (P_0 = 8.3 kPa) while the amplitude of modulation voltage is varied. The variation of the measured pressure $\Delta P/P_0$ in response to the change of modulation depth is plotted in Fig. 6. When the modulation depth is increased from 1.004π to 1.293π (i.e., about 30% of change), the measured pressure is varied with a range of ±3%. It well verifies the

#116807 - $15.00 USD Received 8 Sep 2009; revised 19 Oct 2009; accepted 21 Oct 2009; published 16 Dec 2009

theoretical prediction that the modulation depth does not affect the retrieval of phase as long as it is maintained to be slightly larger than π.

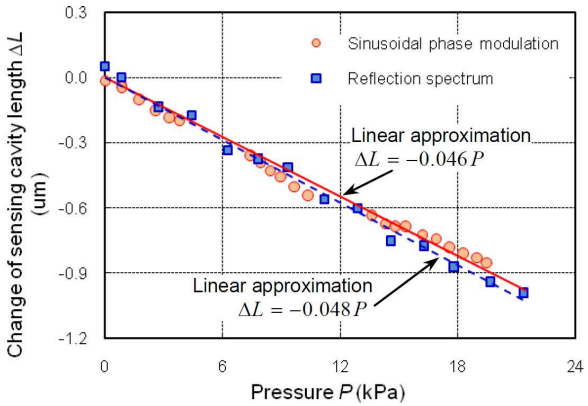

Fig. 5. Comparison of the pressure sensor responses as measured by the sinusoidal modulation scheme and the reflection spectrum method.

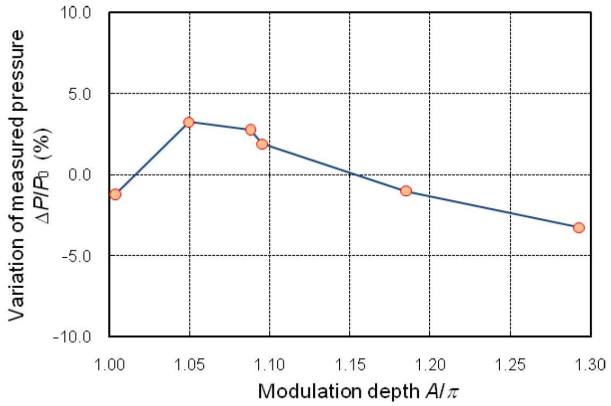

Fig. 6. Variation of the measured pressure in response to the change of modulation depth.

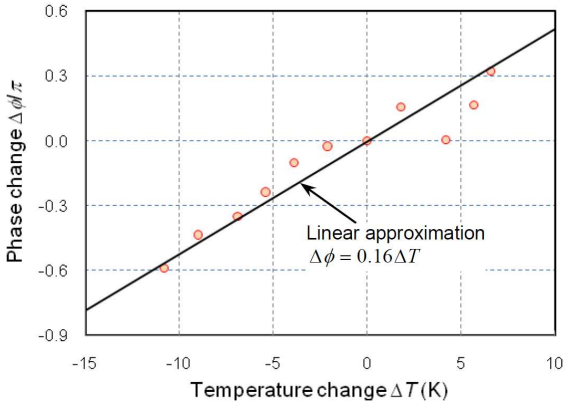

Fig. 7. Variation of the retrieved phase in response to the temperature change.

To examine the reliability of this scheme, the integrated interrogation chip is heated up by a thermal electric cooler (TEC) to simulate the environmental disturbance. The pressure applied to the sensor is maintained constant. The temperature change ΔT with respect to the room temperature is increased from -11 to 7 K. Under the same V_b and V_{s0}, the retrieved phase

#116807 - $15.00 USD Received 8 Sep 2009; revised 19 Oct 2009; accepted 21 Oct 2009; published 16 Dec 2009

experiences an increase with higher temperature as shown in Fig. 7. It follows a linear approximation $\Delta\phi = 0.16\ \Delta T$. Such phase variation might be due to the increase of the comb drive's displacement (i.e., the reference cavity length) when the integrated interrogation chip is heated up. Encapsulation and packaging of the chip would alleviate this problem.

4. Conclusion

We have demonstrated a unique phase modulation scheme for on-chip optical interrogation of low-coherence interferometry based fiber-tip pressure sensors. A phase modulation depth of slightly more than π is produced by the resonant oscillation of a silicon-micromachined curved mirror and gives rise to the appearance of some features such as ditches and humps in the output power waveform. The power levels can be used to retrieve the sensor response in real time using a simple algorithm. This scheme is advantageous over the conventional methods as it avoids the quadrature stabilization, time control, and synchronization and tolerates the modulation signal drift and environmental disturbance.

Appendix

This part will elaborate how to tackle the multi-valued problem of the inverse cosine function in the solutions of ϕ_0' and A based on the prior information that A is slightly larger than π.

Let b_1 and b_2 be the principal values of the inverse cosine functions, i.e.,

$$b_1 = \arccos\frac{2P_{-\pi/2} - P_{\max} - P_{\min}}{P_{\max} - P_{\min}}, \tag{A1}$$

$$b_2 = \arccos\frac{2P_{+\pi/2} - P_{\max} - P_{\min}}{P_{\max} - P_{\min}}. \tag{A2}$$

Here $b_1, b_1 \in [0, \pi]$. For easy discussion, let $a_1 = \pm b_1$ and $a_2 = \pm b_2$. Then, there are

$$A = (m-n)\pi + \frac{1}{2}(a_2 - a_1), \tag{A3}$$

$$\phi_0' = (m+n)\pi + \frac{1}{2}(a_2 + a_1). \tag{A4}$$

Here m and n are integer.

Now it is time to determine the signs of a_1 and a_2 and the values of m and n. In Eq. (A3), the term $(a_2 - a_1)/2$ could have four different forms, $-(b_2 - b_1)/2$, $+(b_2 - b_1)/2$, $-(b_2 + b_1)/2$, $+(b_2 + b_1)/2$. As it is already known that A is slightly larger than π (i.e., $A = \pi + \delta$, here $0 < \delta << \pi$), there are only two situations, one is that the absolute $(b_2 - b_1)/2 = -\pi + \delta, -\delta, \delta$ or $\pi - \delta$; the other is that $(b_2 + b_1)/2 = \delta, \pi - \delta, \pi + \delta$ or $2\pi - \delta$. Based on these conditions, the signs of a_1 and a_2 and the value of (m- n) can be determined. For example, if $(b_2 - b_1)/2 = -\delta$ (the situation in Fig. 4), one can obtain $a_1 = +b_1$, $a_2 = -b_2$ and $(m-n) = 1$. Then ϕ_0' can be determined except for the term of $(m+n)\pi$. Fortunately, the absolute value of ϕ_0' is not very important. Instead, the variation of ϕ_0' with respect to the pressure change is of particular interest. As the term $(m+n)\pi$ acts as a common background for the value of ϕ_0', it can be simply set to be 0 or any other integer.

Although the discussion above is not very rigorous in mathematics, it works well in the experimental implementation. It is worth noting that such sign determination only needs to be done once in the first calculation. The following runs just use the same sign rules, with the utilization of phase unwrapping technique to ensure the continuity of ϕ_0'.

#116807 - $15.00 USD Received 8 Sep 2009; revised 19 Oct 2009; accepted 21 Oct 2009; published 16 Dec 2009

Acknowledgements

We gratefully acknowledge support from Air Force Office of Scientific Research (Grant No. FA95500810042) and Center for Rotorcraft Innovations (National Rotorcraft Technology Center Research Program under the agreement of AATD TIA W911W6-06-2-0002).

#116807 - $15.00 USD Received 8 Sep 2009; revised 19 Oct 2009; accepted 21 Oct 2009; published 16 Dec 2009